Supplemental Document

Reconfigurable photon localization by coherent drive and dissipation in photonic lattices: supplement

O. Jamadi,[1,†,5] B. Real,[1,†] K. Sawicki,[2] C. Hainaut,[1] A. González-Tudela,[3] N. Pernet,[4] I. Sagnes,[4] M. Morassi,[4] A. Lemaître,[4] L. Le Gratiet,[4] A. Harouri,[4] S. Ravets,[4] J. Bloch,[4] and A. Amo[1,*]

[1] *Univ. de Lille, CNRS, UMR 8523–PhLAM–Physique des Lasers, Atomes et Molécules, Lille, France*
[2] *Institute of Experimental Physics, Faculty of Physics, University of Warsaw, Pasteura St. 5, 02-093 Warsaw, Poland*
[3] *Institute of Fundamental Physics IFF-CSIC, Calle Serrano 113b, 28006 Madrid, Spain*
[4] *Université Paris-Saclay, CNRS, Centre de Nanosciences et de Nanotechnologies, 91120, Palaiseau, France*
[5] *e-mail: omar.jamadi@gmail.com*
[†] *These authors contributed equally to this paper.*
[*] *Corresponding author: alberto.amo-garcia@univ-lille.fr*

Supplement DOI: https://doi.org/10.6084/m9.figshare.19678944

Parent Article DOI: https://doi.org/10.1364/OPTICA.452624

Reconfigurable photon localization by coherent drive and dissipation in photonic lattices

O. JAMADI,[1,5,†] B. REAL,[1,†] K. SAWICKI,[2] C. HAINAUT,[1] A. GONZÁLEZ-TUDELA,[3] N. PERNET[4], I. SAGNES[4], M. MORASSI[4], A. LEMAÎTRE[4], L. LE GRATIET[4], A. HAROURI[4], S. RAVETS[4], J. BLOCH[4] AND A. AMO[1,*]

[1]*Université de Lille, CNRS, UMR 8523 – PhLAM – Physique des Lasers, Atomes et Molécules, Lille, France*

[2]*Institute of Experimental Physics, Faculty of Physics, University of Warsaw, Pasteura St. 5, 02-093 Warsaw, Poland*

[3]*Institute of Fundamental Physics IFF-CSIC, Calle Serrano 113b, 28006 Madrid, Spain.*

[4]*Université Paris-Saclay, CNRS, Centre de Nanosciences et de Nanotechnologies, 91120, Palaiseau, France*

[5]*omar.jamadi@gmail.com*
**alberto.amo-garcia@univ-lille.fr*

[†]*This authors contributed equally to this Article*

Supplementary information

Sample description.

The microcavity used for these studies was fabricated by molecular beam epitaxy. The heterostructure is made of two Bragg mirrors of 28 (top) and 32 (bottom) pairs of alternating layers of $Ga_{0.90}Al_{0.10}As$ and $Ga_{0.05}Al_{0.95}As$ of thickness $\lambda/4$, embedding a λ spacer of GaAs, with λ = 880 nm/n, and n being the index of refraction of the material of each layer at 6K. A single $In_{0.09}Al_{0.91}As$ quantum well of 20 nm in width is grown at the centre of the cavity spacer. The whole heterostructure is grown on an epitaxial quality GaAs substrate. During the growth of the Bragg mirrors and the cavity spacer the substrate was not rotated. Due to the flux angle of the different material cells in the growth chamber with respect to the substrate, the cavity and mirrors present a wedge across the wafer. In this way, different points of the wafer have different thicknesses and different cavity-mode energies. In the reported experiments we select a point of the wafer in which the lowest photonic modes is red-detuned by 18 meV from the quantum well exciton resonance (at 1.4099meV at 6K, the temperature of our experiments). This detuning is much larger than half the Rabi splitting 3.5meV/2=1.75meV. In this way, any polaritonic effect can be neglected in the present experiments and all our data imply bare photons. By selecting a different point of the sample with a smaller photon-exciton detuning, it would be possible to work with polaritons with higher excitonic content and address, for instance, nonlinear effects.

The as-grown planar structure is then processed with electron beam lithography and it is etched down to the substrate (Inductively Coupled Plasma Etching). By properly designing the electron beam mask, we fabricate honeycomb lattices of coupled round micropillars with

2.75 μm diameter and a centre-to-centre separation of 2.3 μm. In the lattices considered in this work, the photon lifetime is estimated to be 9 ps. This value is obtained from fitting simulations of Eq. (1) in the conditions of the experiment to the observed propagation patterns in Fig. 2(c) in the main text.

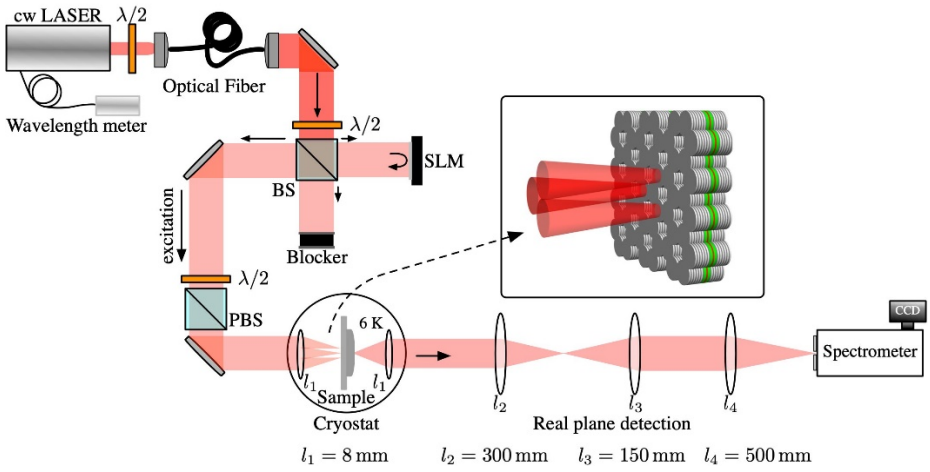

Fig. S1. Scheme of the experimental setup.

Experimental setup.

Figure S1 shows a scheme of the experimental setup. The sample with the lattice of micropillars is held in vacuum inside a closed-cycle He cryostat at a temperature of 6K as measured on the sample holder. The excitation beam is a Ti:Sapph single mode laser (<10MHz linewidth) which passes through a single-mode polarisation maintaining fibre to obtain a clean Gaussian mode. After the fibre, the beam goes through a spatial light modulator in reflexion geometry, a telescope (not shown in the figure) and the excitation lens, which allow engineering the excitation pattern in the form of one, three or more spots on the surface of the lattice. The experiment is done in transmission geometry: the excitation beam impinges the sample through the epitaxial side, traverses the substrate, passes through a slit of 3 mm width in the sample holder and exits the cryostat towards the collection optics. Both for excitation and detection we use 8 mm focal length aspherical lenses with numerical aperture 0.5. Note that the GaAs substrate is transparent with negligible absorption at the wavelength of this work.

After being collected by the collection lens, the emitted light is imaged onto a CCD and a spectrometer. The excitation is vertically polarised and detection is done along the same polarisation axis.

Simulations.

The numerical simulations of Eq. (1) displayed throughout the article have been realized using the split-step method after switching on the excitation field in a step function. We wait long enough to obtain the steady state response. To display the result of the simulations in space, each point of the lattice shows the amplitude square of the fundamental Laguerre-Gauss mode with a Full Width at Half Maximum of 2.4 μm, with a peak intensity given by the simulation.

Theoretical analysis of localisation by drive and dissipation in a 1D lattice

To get an intuitive understanding of the nature of the localisation of the emission in the polariton lattices subject to drive and dissipation, we analyse the driven-dissipative Schrödinger Eq. (1) in the main text:

$$i\hbar\frac{\partial\psi_m}{\partial t} = \varepsilon_m\psi_m + \sum_n t_{m,n}\psi_n - i\frac{\hbar}{\tau}\psi_m + F_m e^{-i\omega_p t}. \quad \text{(S1)}$$

ψ_m is the field amplitude at the centre of micropillar m, $\varepsilon_m = E_0$ is the energy of the lowest energy mode in each pillar –assumed to be identical for all sites–, $t_{m,n}$ is the coupling amplitude between different sites of the lattice, τ is the photon radiative lifetime, and F_m is the complex amplitude of the resonant excitation laser at site m with photon energy $\hbar\omega_p$.

In the rotating frame of the pump frequency ω_p, in the limit of losses much weaker than the hopping (i.e., $\frac{\hbar}{\tau} \ll t_{m,n}$), the term $-i\frac{\hbar}{\tau}\psi_m$ can be neglected and the steady state of Eq. (1) takes the simple form:

$$\Delta\psi_m + \sum_n t_{m,n}\psi_n = -F_m, \quad \text{(S2)}$$

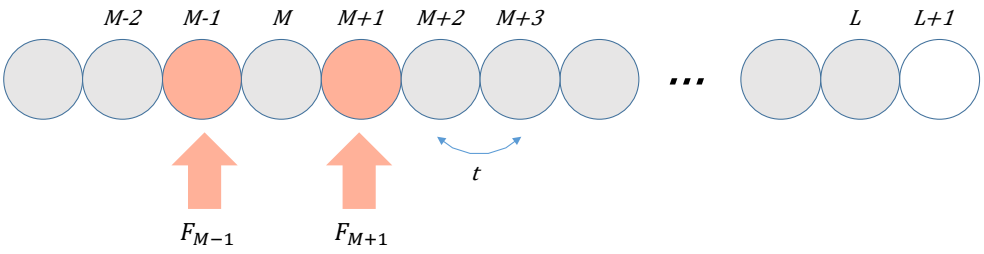

Fig. S2. Schematic representation of a one-dimensional lattice with two pump drives at sites $M-1$ and $M+1$. The site $L+1$ is out of the lattice.

where $\Delta = E_0 - \hbar\omega_p$ is the detuning between the onsite energy and the pump frequency. We consider the case of a one-dimensional lattice with nearest-neighbour hoppings in the configuration described in Fig. 1(b) and S2, with pumps at lattice sites $M-1$ and $M+1$ with drive of amplitudes F_{M+1} and F_{M-1}.

We can explicitly write Eq. (S2) for a few sites at an around the pumps:

$$\text{site } M: \quad \Delta\psi_M + t(\psi_{M-1} + \psi_{M+1}) = 0 \quad \text{(S3)}$$

$$\text{site } M-1: \quad \Delta\psi_{M-1} + t(\psi_{M-2} + \psi_M) = -F_{M-1} \quad \text{(S4)}$$

$$\text{site } M+1: \quad \Delta\psi_{M+1} + t(\psi_M + \psi_{M+2}) = -F_{M+1} \quad \text{(S5)}$$

$$\text{site } M+2: \quad \Delta\psi_{M+2} + t(\psi_{M+1} + \psi_{M+3}) = 0 \quad \text{(S6)}$$

$$\text{site } M+3: \quad \Delta\psi_{M+3} + t(\psi_{M+2} + \psi_{M+4}) = 0 \quad \text{(S7)}$$

$$\text{site } M+4: \quad \Delta\psi_{M+4} + t(\psi_{M+3} + \psi_{M+5}) = 0 \quad \text{(S8)}$$

$$\text{site } M+5: \quad \Delta\psi_{M+5} + t(\psi_{M+4} + \psi_{M+6}) = 0 \quad \text{(S9)}$$

Let us look for solutions for which the pumped sites $M \pm 1$ have zero amplitude ($\psi_{M-1} = \psi_{M+1} = 0$). From Eq. (S3) we see that this implies that $\Delta = 0$. From Eq. (S6) we see that if $\Delta = 0$ and $\psi_{M+1} = 0$, then ψ_{M+3} must be zero. Subsequently, Eq. (S8) implies that $\psi_{M+5} = 0$ and this happens for all the sites $m = M \pm (2n + 1)$, for $n = 1, 2, 3,...$ Therefore, all sites separated by an odd number of pillars from the central site M must have zero amplitude.

We will see now that this is the case also for sites separated by an even number of pillars from the central site M. From Eq. (S7) and (S9) with $\Delta = 0$, we see that $\psi_{M\pm 2n} = \psi_{M\pm(2n+2)}$. Consequently, all these sites have the same amplitude. We can see that their amplitude must be zero using the following argument: let us assume that the last site of the lattice, L, is separated by an odd number of pillars. Then, the site $L + 1$, which actually does not exist, can be described by imposing its amplitude to be zero [1]: $\psi_{L+1} = 0$. Therefore, all the series of sites $\psi_{M\pm 2n}$ to which it belongs are also zero.

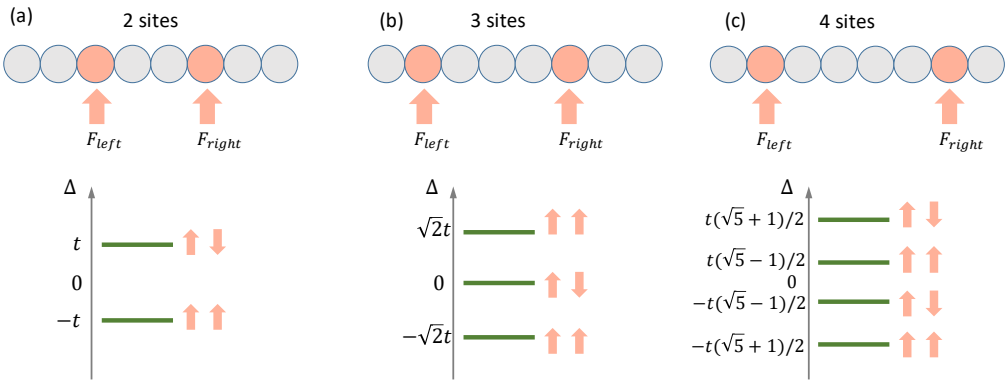

Fig. S3. Scheme for the generation of localised modes in larger chain sections, when the driving pumps are separated by 2, 3, and 4 sites in, (a), (b), and (c), respectively. The lower panels show the resonant driving frequencies of the localised modes. They correspond to the eigenenergies of 2, 3 and 4 coupled sites, respectively. The arrows indicate the relative phase of the pumps to excite each respective mode (up-up are in-phase pumps, up-down are out-or-phase pumps).

To calculate the amplitude in the central site M we focus on Eqs. (S4) and (S5). As we have just seen, if $\Delta = 0$ there is a solution to the set of coupled Eqs. (S2) in which all sites except for ψ_M are zero. Inserting $\psi_{M+1} = \psi_{M-1} = 0$ in Eqs. (S4) and (S5) we directly see that $\psi_M = -F_{M-1}/t = -F_{M+1}/t$: the pump spots on the two sites surrounding M must have equal amplitude and phase for the destructive interference effect away from M to take place. The amplitude at ψ_M is directly proportional to the pump amplitude.

Multiple sites

The interference of the pump fields in the lattice has a double effect. First, from the previous example, we see that the search for solutions in which the pumped sites have zero amplitude implies that the frequency of the pump must coincide with the eigenenergies of the site surrounded by the pumped sites, as if it was detached from the lattice. Second, the condition that the pumped sites have zero amplitude implies that the amplitude is zero everywhere else in the lattice except from the sites surrounded by the pumps.

We can extend this argument to situations in which the pumps are separated by more than two sites. Figure S3 shows several cases along with the pump energies at which modes entirely localised in between the pump spots are found. When the region in-between pumps is made of two sites (Fig. S3(a)), the localised modes appear at frequencies Δ corresponding to the eigenmodes of two coupled isolated sites: $\Delta = -t$ and $\Delta = +t$. The amplitude and phase of the two pumps must respect the phase distribution of the isolated modes at the edges: for $\Delta = -t$ (bonging mode) $F_{left} = F_{right}$, for $\Delta = t$ (antibonging mode) $F_{left} = -F_{right}$. Note that this situation is very similar to the case reported in Fig. 3 of the main text for two pillars in a honeycomb lattice.

If the region in-between pumps is larger, more localised resonances appear (see Fig. S3(b)-(c)), with frequencies given by the eignemodes of the region in-between the pumps as if it was detached from the lattice.

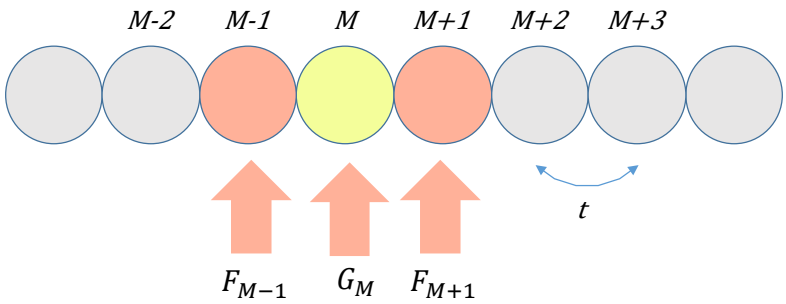

Fig. S4. Schematic representation of a one-dimensional lattice with two pump drives at sites $M-1$ and $M+1$ and an additional drive at site M.

Shift of the energy of the localisation resonance

Figure 4 in the main text shows that the drive frequency of the localisation resonance at a single site can be shifted at will by adding an extra drive on top of the localisation site. In the main text we have proved this feature numerically for the conditions of Fig. 4. To get further insights, we now consider the one-dimensional lattice of Fig. S4 and Eqs. (S3)-(S9). We treat the case in which $F_{M-1} = F_{M+1} = F$ and we add an additional pump of same photon energy $\hbar\omega_p$ and amplitude G_M to the site surrounded by the two pumps F. As mentioned in the main text, we anticipate that this situation will modify the photon energy at which the perfect localisation condition takes place. In the present case, all equations (S3) to (S9) remain the same except for Eq. (S3), which becomes:

$$\text{site } M: \qquad \Delta\psi_M + t(\psi_{M-1} + \psi_{M+1}) = -G_M \qquad \text{(S3')}$$

If we now impose the condition $\psi_{M-1} = \psi_{M+1} = 0$, we see that $\psi_M = -G_M/\Delta$. Inserting this into Eq. (S5) gives:

$$G_M = \frac{F_{M+1}\Delta}{t} + \psi_{M+2}. \qquad \text{(S10)}$$

We now look for the condition that ψ_{M+2}, which is out of the region in-between the pumped spots, is zero. This imposes a value of the drive detuning:

$$\Delta = t\frac{G_M}{F_{M+1}} = t\frac{G_M}{F} \qquad \text{(S11)}$$

For that value of the drive detuning with respect to the energy of an isolated micropillar, the fields at the sites under the external pumps $M \pm 1$ and at site $M + 2$ are zero. The same argument using Eq. (S4) shows that the field is also zero at $M + 2$. Now, using the recurrent equations (S6), (S7), (S8), … we can see that, for the similar reasons as in the previous example, the amplitude ψ_m all sites with $m > M + 1$ and $m < M - 1$ must be zero.

Equation (S11) thus shows that the photon energy $\hbar\omega_p = \Delta + E_0$ of the driving field at which localisation takes place in a single site can be modified by adding an extra laser of amplitude G_M at the site surrounded by the main driving fields. If the extra laser is in phase with the pumps F ($G_M > 0$), the resonance condition moves to higher Δ, that is, to higher laser frequency energies. While an out of phase field ($G_M < 0$) shifts the resonance condition to lower energies. The additional field G_M acts as a renormalized onsite energy for the isolated site.

Extension to 2D lattices

The previous discussion aims at providing intuitive insights on the interference process at the core of the localisation phenomena we report. We have treated the simple case of a one-dimensional lattice with simple pump configurations. We anticipate that these results can be extrapolated to other pump configurations and to higher dimensional lattices. Several examples including a square lattice and a honeycomb lattice are treated in the main text.

In the present work we have considered situations in which the pump spots surround the region in which localisation resonances takes place. It would be interesting to explore other situations that go beyond this geometry. For instance, recent theoretical studies of the behaviour of a quantum emitter in a photonic lattice show that just a few number of emitters cleverly placed can confine light in large areas of the lattice [2–6]. Even a single emitter close to a corner of a two-dimensional lattice has been shown to do this [5]. The similarity between the two systems (the role of the emitters is here played by the resonant drives) anticipates interesting perspectives for our all-optical configuration.

Role of lifetime

The simple analytical model we have developed above for a one-dimensional lattice assumed that photon the photon loss rate was much smaller than the hopping amplitude. This situation results in perfect destructive interference effects at and away from the pumped spots. If photon losses are significant, the interference from the fields injected by the different pumps is not perfect and localisation is degraded. Nevertheless, the robustness of the localisation phenomenon to short lifetimes is remarkable, particularly when the considered geometry involves spots that are not too far apart. Figure S5 shows, for the geometry of three pumped sites of Fig. 2(d) of the main text, the calculated IPR at $\hbar\omega_p = E_0$ as a function of the photon losses τ. In the limit of very large losses ($\tau \to 0$) we obtain an IPR of 0.33. This is a consequence of the fact that we chose to illuminate the sample with three spots and that the light is immediately radiated before having the time to hop to the neighbouring sites. When increasing the lifetime progressively, photons have the time to go through a first hopping event and, as the initial phase of the three pumps is the same, they interfere constructively in the centre. This situation is depicted in the left inset of Fig. S5, which shows that the population is now split over 4 pillars leading to an IPR smaller than 0.33 for small but non-zero lifetime. Increasing even more the lifetime allows the light to realize larger path loops in the lattice and destructive interference effects at the pump spots set-in. Simultaneously, the population increases dramatically at the center pillar, where the interferences are constructive. In this case the IPR reaches very high values of up to 0.9 (see right inset of Fig. S5). We can see that the limitation

of the maximal IPR value observed in this configuration (solide blue line) comes from the presence of next-nearest neighbour interactions. When next-nearest neighbour hopping is suppressed (dashed blus line), the IPR asymptotically reaches the value of one at very long lifetimes.

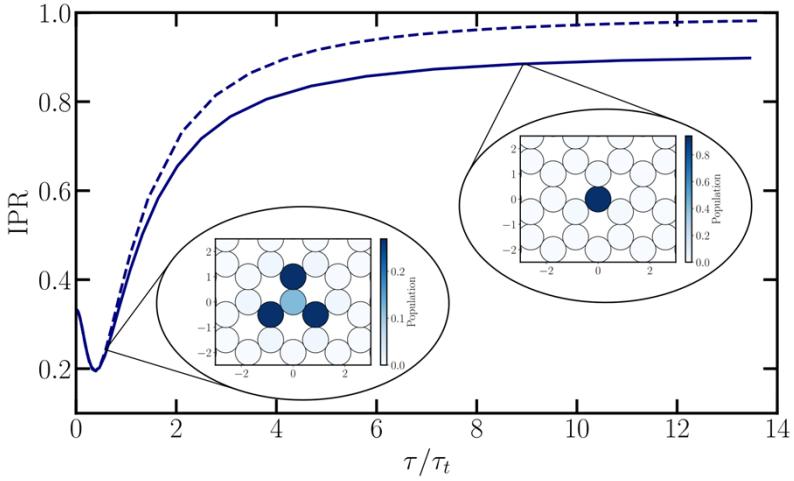

Fig. S5. Calculated value of the IPR peak at $\hbar\omega_p = E_0$ as a function of the photon lifetime τ in the conditions of Fig. 2(d). The dashed curve is calculated without next-nearest-neighbour coupling while the solid one takes it into account using the values of the main text: nearest-neighbour coupling $t = 0.328$ meV, next-nearest-neighbour coupling $t' = 0.042$ meV. The typical time associated to the nearest-neighbour hopping is $\tau_t = \hbar/(2t)$. The insets show the calculated populations of the real space patterns at selected values of lifetime (0.25ps and 9ps).

Investigation of the anti-bonding scenario

Figure S6 presents an investigation of the scenario where four pump spots of equal amplitude are used, and where the upper two spots have a phase difference of π with respect to the lower two spots. This specific configuration, where the phase is experimentally controlled with a SLM, allows to excite the anti-bonding mode of the two coupled sites molecule which is expected at a photon energy $E \approx E_0 + t$. The measured IPR (bottom panel) presents a peak at $E = E_0 + 0.221$ meV. The real space emission at that energy (top panel) clearly shows localisation in the two pillars surrounded by the four pumps. The anti-bonding character of this mode can be identified from the node in the emission at the boundary between the two pillars, which is expected if the upper and lower emit with a phase difference of π. The low value of the measured IPR peak and the presence of a peak at around $E = E_0 - 0.4$ meV (close to the bonding mode) suggest that the actual phases of the excitation spots depart from the nominal value.

Figure S5(b) shows the calculated IPR as a function of photon energy for perfect alignment conditions (bottom panel). An IPR peak is visible at $\hbar\omega_p = E_0 + 0.251$ meV. This value deviates from the antibonding energy of the two coupled isolated micropillars $\hbar\omega_p = E_0 + t$ (recall that $t = 0.328$ meV) due to the next-nearest-neighbour hopping included in our model ($t' = 0.042$ meV). The field amplitude at the energy corresponding to the peak of the IPR is shown in the upper panel and evidences the anti-bonding nature of the localised mode.

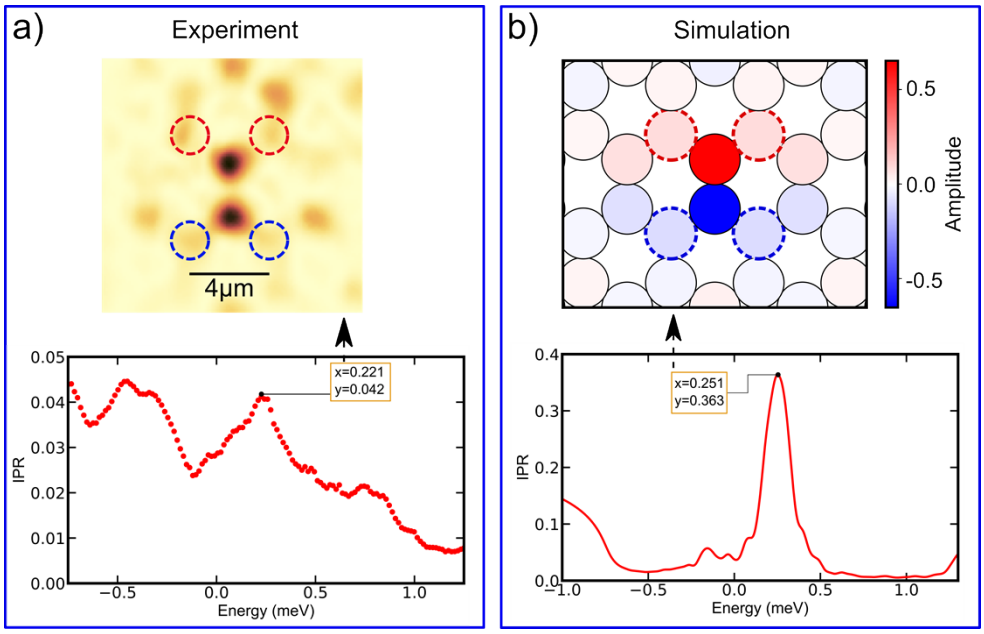

Fig. S6. (a) Top: Measured real space emission pattern at photon energy $E = E_0 + 0.221$ meV for excitation with four pump spots located at the sites marked with dashed lines. Nominally, upper and lower spots present a phase difference of π. Bottom: measured IPR as a function of the laser frequency. E_0 has been artificially shifted to zero. (b) Top: Calculated field amplitude distribution at each lattice site for the driving energy corresponding to the IPR peak at $E = E_0 + 0.251$ meV. Bottom: Calculated IPR as function of the photon energy.

Effects of disorder

The effect of disorder on the localisation of light is shown in Fig. S7 for the case of three spot excitation. The figure shows the numerically calculated IPR in the conditions of Fig. 2(d),(g). The red dashed lines depict the IPR in the absence of any disorder, same phase for three spots and a photon lifetime of 9 ps. The solid lines show the calculated IPR for three different realisations of disorder in the onsite energies (a) and in the hoppings (b). In (a) the value of each onsite energy is varied randomly between $E_0 - t$ and $E_0 + t$, where E_0 is the energy of the central site surrounded by the three pump spots. In (b) each nearest neighbour hopping amplitude was randomly varied between $0.75t$ and $1.25t$. In both cases the IPR shows a very high peak value, attesting a high degree of localisation, and a very similar width.

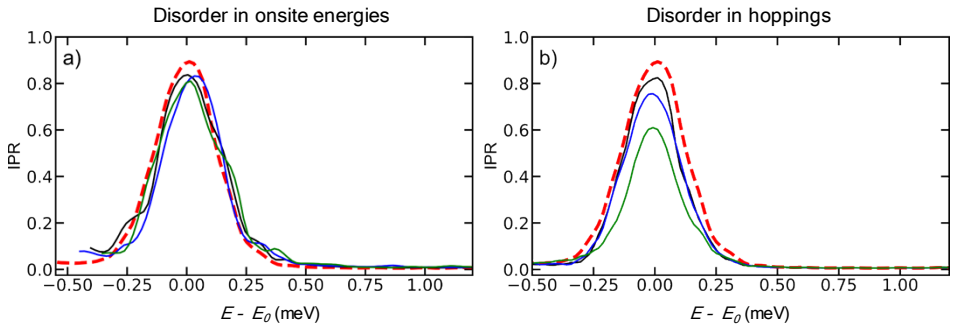

Fig. S7. (a) Top: Measured real space emission pattern at photon energy $E = E_0 + 0.221$ meV for excitation with four pump spots located at the sites marked with dashed lines. Nominally, upper and lower spots present a phase difference of π. Bottom: measured IPR as a function of the laser frequency. E_0 has been artificially shifted to zero. (b) Top: Calculated field amplitude distribution at each lattice site for the driving energy corresponding to the IPR peak at $E = E_0 + 0.251$ meV. Bottom: Calculated IPR as function of the photon energy.

References

1. P. Delplace, D. Ullmo, and G. Montambaux, "Zak phase and the existence of edge states in graphene," Physical Review B **84**, 195452 (2011).
2. A. González-Tudela and J. I. Cirac, "Quantum Emitters in Two-Dimensional Structured Reservoirs in the Nonperturbative Regime," Phys. Rev. Lett. **119**, 143602 (2017).
3. A. González-Tudela and J. I. Cirac, "Markovian and non-Markovian dynamics of quantum emitters coupled to two-dimensional structured reservoirs," Phys. Rev. A **96**, 043811 (2017).
4. A. González-Tudela and J. I. Cirac, "Exotic quantum dynamics and purely long-range coherent interactions in Dirac conelike baths," Phys. Rev. A **97**, 043831 (2018).
5. A. Feiguin, J. J. García-Ripoll, and A. González-Tudela, "Qubit-photon corner states in all dimensions," Phys. Rev. Research **2**, 023082 (2020).
6. L. Leonforte, A. Carollo, and F. Ciccarello, "Vacancy-like Dressed States in Topological Waveguide QED," Phys. Rev. Lett. **126**, 063601 (2021).